Available online at www.sciencedirect.com
ScienceDirect
Coordination Chemistry Reviews 251 (2007) 2510–2521
COORDINATION CHEMISTRY REVIEWS
www.elsevier.com/locate/ccr

Review

# Observation of gas molecules adsorbed in the nanochannels of porous coordination polymers by the *in situ* synchrotron powder diffraction experiment and the MEM/Rietveld charge density analysis

Yoshiki Kubota [a,*], Masaki Takata [b], Tatsuo C. Kobayashi [c], S. Kitagawa [d]

[a] *Department of Physical Science, Graduate School of Science, Osaka Prefecture University, Sakai, Osaka 599-8531, Japan*
[b] *Structural Science Laboratory, Harima Institute SPring-8 Center, RIKEN and CREST, Japan Science and Technology Agency, Sayo-gun, Hyogo 679-5198, Japan*
[c] *Department of Physics, Okayama University, Okayama 700-8530, Japan*
[d] *Department of Synthetic Chemistry and Biological Chemistry, Graduate School of Engineering, Kyoto University, Katsura, Kyoto 615-8510, Japan*

Received 31 December 2006; accepted 27 July 2007
Available online 8 August 2007

## Contents



**Abstract**

Microporous coordination polymers have attracted attention for their numerous nanotechnology and engineering applications. Nano-coordination space provides some unique properties and functions that could never be realized in conventional porous materials. For the strategy of rational designs and the syntheses of novel porous coordination polymers, the structural information of adsorbed guest molecules inside the nanopores and the host framework is very important. In the present study, we describe the technique of the direct observation of gas molecules adsorbed in the nanochannels of porous coordination polymers by the *in situ* synchrotron powder diffraction measurement of gas adsorption and the maximum entropy method (MEM)/Rietveld charge density analysis. Specific alignment and properties of molecular oxygen obtained by gas adsorption in the nano-coordination space are revealed.


*Keywords:* Porous coordination polymers; Gas adsorption; Structure analysis; Synchrotron powder diffraction; Charge density; Maximum entropy method

## 1. Introduction

A porous coordination polymer is a crystalline material, which is formed by the coordination bonds between transition metal cations and bridging organic ligands by a self-assembly mechanism. Metal cations have characteristic directional coordination geometries. Organic ligands provide building components of various sizes and shapes. These elements form uniformly ordered nanopore structures of various sizes and shapes [1,2]. These materials are synthesized with a solvent or water molecules inside the nanopores. In order to utilize their nanopores, the guest molecules must be removed

* Corresponding author. Tel.: +81 72 254 9193; fax: +81 72 254 9931.
*E-mail address:* kubotay@p.s.osakafu-u.ac.jp (Y. Kubota).

0010-8545/$ – see front matter © 2007 Elsevier B.V. All rights reserved.
doi:10.1016/j.ccr.2007.07.025

from the pores. In the 1990s, porous coordination polymers with stable framework structures after the removal of guest molecules were synthesized [3–5], and the investigation of these materials using nanopores has continued. Porous coordination polymers have a very large surface area of nanopores of over a few thousand $m^2\ g^{-1}$. If the size of the pores is close to that of the guest molecules, then the guest molecules are strongly affected by the pores. By the overlapping of the potentials of pore walls, the van der Waals force with very weak interaction is no longer negligible for the thermal energy of molecules. Therefore, these materials show very good sorption properties and are promising as gas storage materials of energy gases such as hydrogen, methane, and oxygen. These materials have unique properties besides the gas sorption properties, which are different from those of conventional porous materials such as zeolites and activated carbon. These properties include flexibility of framework, due to the coordination bonds and the degree of freedom in organic molecules, and the functionalities added to the nanopores by the chemical modification. One of the most important properties of these materials is that the frameworks with various types of nanopore structures can be designed and synthesized by the combination of metal cations and bridging ligands. Recently, novel functionalities revealed by the introduction of guest molecules have attracted attention, and a variety of applications, including gas storage [6–10], anion exchange [11], and heterogeneous catalysis [12], are expected. The syntheses and applications of porous coordination polymers have been studied extensively. In particular, the gas adsorption properties have been actively investigated. In these studies, the amounts of adsorbed molecules, the pore surface areas, and the physicochemical properties have been discussed based on the gas adsorption isotherm. In the structural investigation, the X-ray diffraction pattern is compared with the simulated pattern calculated from the estimated crystal structure, and the structural transformation is estimated from the change of lattice parameters. Direct information of the adsorbed gas molecules, that is, the position and orientation in the nanochannels and the intermolecular interaction between the guest gas molecules and host frameworks have not yet been revealed. Such fundamental structural information of guest molecules and the host framework is required for the rational design and syntheses of novel porous coordination polymers as functional materials. This information is also important for an in-depth understanding of gas adsorption phenomena and the unique physical and chemical properties in these materials.

As shown previously, porous coordination polymers are crystal materials with uniformly ordered nanochannels. If the guest molecules form an ordered structure inside the nanopores, the formation will likely be observed by the diffraction method, and we can examine the arrangement of adsorbed gas molecules. Electron microscope observation is a direct method by which to observe the framework structures and is widely applied to the observation of porous materials like zeolites. However, electron microscope observation generally cannot be applied to the observation of gas-adsorbed materials because the environment of a sample is a vacuum. X-ray diffraction is a very powerful method for the structural determination of crystal materials. The introduction of the third-generation synchrotron radiation light source has also provided much higher resolution and higher counting statistic diffraction data, as compared to the laboratory source. Using a high-brilliance light source, an *in situ* diffraction experiment of gas adsorption can be performed with small amounts of samples.

The maximum entropy method (MEM) is a type of deconvolution method that was developed in the field of information theory. In crystal structure analysis, the high-resolution charge density distribution can be obtained from a limited number of structure factors [13,14]. Imaging of the charge density by the MEM combined with the powder pattern decomposition of the Rietveld method [15,16] enables a structural model of the gas-adsorbed phase, which is not easily estimated at the initial stage of analysis without any information on the guest molecules, to be built. Furthermore, the obtained charge density provides information of the intermolecular interaction between the adsorbed gas molecules and the host framework.

In the present review, we intend to show the method by which to observe the gas molecules adsorbed in the nanochannels of porous coordination polymers by the MEM/Rietveld method using the third-generation synchrotron powder diffraction data and discuss the alignment and specific state of the molecular oxygen in the nano-coordination space [17].

## 2. *In situ* synchrotron powder diffraction experiment of gas adsorption

*In situ* X-ray diffraction data of gas adsorption were measured by a powder method. One reason to apply a powder method is to avoid difficulties related to the collapse of a single crystal by the large volume change in the guest adsorption and desorption. In particular, in materials with nanochannel structure, homogeneity of the adsorption state within the crystals is required because the entrances of the nanochannel may be blocked to avoid diffusion of guest molecules into the crystals. In the powder diffraction method, the integrated intensities of diffraction peak are calculated by the kinematical theory, and the extinction correction for the intensities is virtually negligible. The correction for the absorption of the sample is easily and accurately carried out. In order to obtain reliable data, it is very important for the charge density analysis to avoid, to the extent possible, any corrections. These are the advantages of a powder method as compared to the single-crystal diffraction method.

An *in situ* synchrotron powder diffraction experiment of gas adsorption was carried out at the beamline BL02B2 SPring-8 [18]. An incident X-ray beam from the bending magnet was monochromatized by silicon (1 1 1) double crystals. The beam was focused vertically and the higher order reflections from the monochromator crystals were removed by a mirror before reaching the monochromator. The beam was collimated to 0.5 mm (V) × 2.0 mm (H). A diffractometer installed in the beamline is a type of a Debye–Scherrer camera with a radius of 287 mm. An imaging plate (IP) of 400 mm × 200 mm was used as a detector covering the range from 0° to approximately 70° in $2\theta$. One pixel of the IP corresponds to 0.01° in $2\theta$. A slit with a width of 10 mm was placed in front of the IP. Multiple data (ex. the

variation of the temperature dependence) can be recorded on the same IP. The two-dimensional intensity distribution of the Debye–Scherrer ring can be observed, and the uniformity of the particle size is easily assessed.

One way to examine various adsorption states is to measure a number of capillary samples sealed with different gas pressures. However, measurement with the same sample is best in order to avoid a dependency on sample and ambiguities for conditions other than the controllable parameters. In order to perform an *in situ* measurement in the gas adsorption state, a sample holder and a gas handling system were constructed and equipped with the standard experimental settings in the beamline. The sample cell must isolate the powder sample from the ambient atmosphere. The temperature and gas pressure must be controlled to obtain various adsorption states. With a length of approximately 2 mm, the powder sample is enclosed by a thin-walled glass capillary. The size of the capillary is determined based on the relationship between the absorption of the sample material and the energy of an X-ray. We usually generate conditions such that the dependence of the absorption factor on the diffraction angle is negligible. Under such conditions, the difference of absorption factors within the observed range of from 0° to 70° is less than 1%. In a typical case for the porous coordination polymers, the size of the capillary is 0.4 mm with an inner diameter for the wavelength of an incident X-ray of 0.8 Å. The capillary containing the powder specimen was attached to the stainless steel tube using an epoxy adhesive. The capillary was mounted to the custom sample holder, which was constructed from Swagelok parts and steel tube, for the gas introduction. A stainless steel tube attached to the sample holder was connected to the gas handling system with a number of valves and a pressure gauge. A helium leak detector is connected to the system for the evacuation and vacuum leak check. A gas bottle of adsorbate is also connected to a gas handling system. During the measurement, the capillary sample was oscillated approximately 30° in order to obtain a uniform distribution of intensities of a Debye–Scherrer ring. The temperature of the sample was controlled by a high and low temperature nitrogen gas blower. The temperature range was controlled to be from 90 to 1000 K. Using this system, the measurement is carried out under approximately the same condition as the standard measurement in this beamline. A schematic diagram and photographs of this system are shown in Fig. 1. In the Debye–Scherrer camera method, all reflections are simultaneously measured under the same conditions. The data is not affected by trivial changes or decay of the intensity of the incident X-ray beam. In addition, there are few moving parts during the measurement. These are great advantages for *in situ* measurement. Accordingly, the measurement time is very long, as compared to the step scan method. A 1-h measurement provides each data point with the intensity of the counting statistics for one hour. As a result, a very high-counting statistic is obtained for powder diffraction data. This is one of the most important factors in accurate charge density analysis.

We next describe the procedure of an *in situ* powder diffraction experiment with the adsorption of oxygen on a type of copper coordination polymer as an example. The sample used here is $[Cu_2(pzdc)_2(pyz)]_n$ (pzdc: pyrazine-2,3-dicarboxylate,

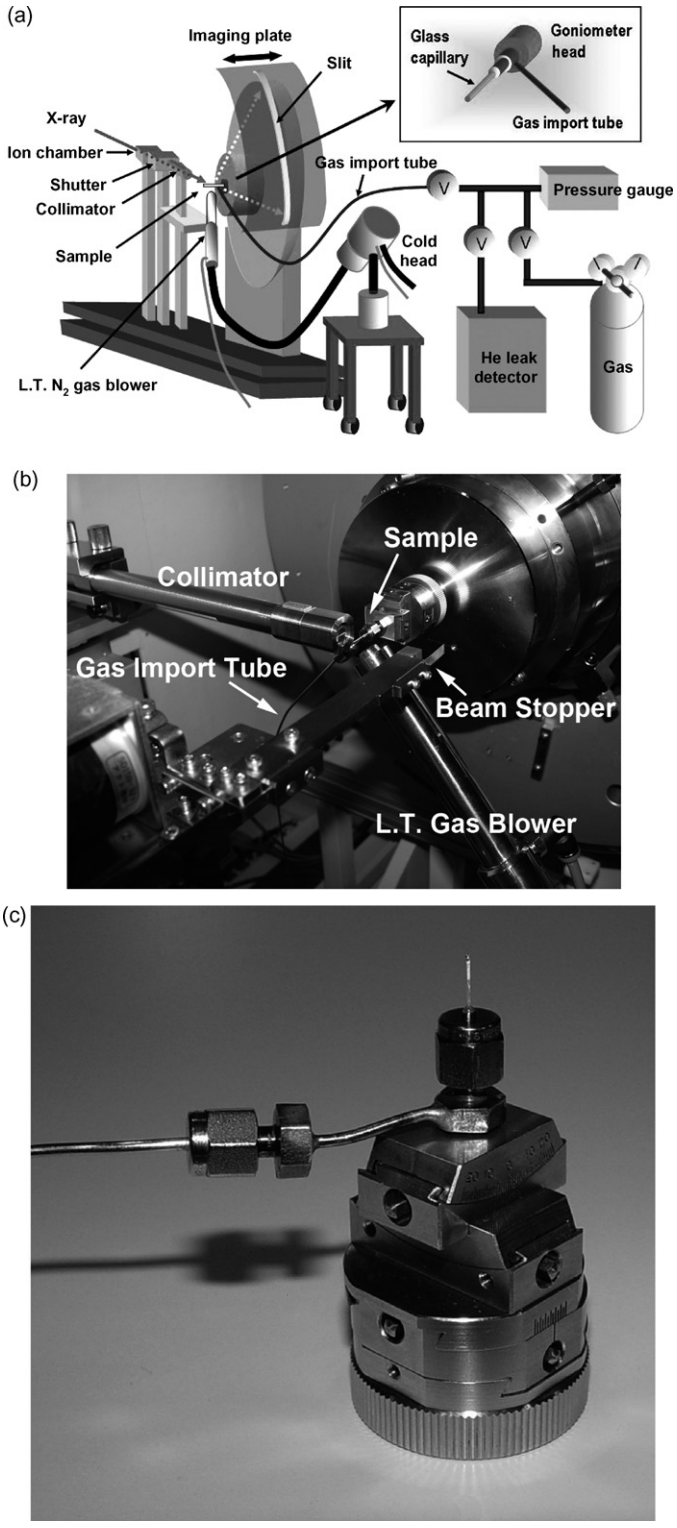


Fig. 1. (a) Schematic diagram of the system used to conduct the *in situ* powder experiment of gas adsorption at BL02B2 SPring-8, (b) is a photograph of the area around the sample during measurement, and (c) is a photograph of the sample holder with a gas import tube.

pyz: pyrazine) called CPL-1 (Coordination polymer 1 with a pillared-layer structure) with uniform nanochannels of 4 Å × 6 Å [3]. The sample holder is mounted to the goniometer head of the diffractometer and the gas import tube is connected to a gas handling system. The atmosphere inside the capillary is evacuated, and a helium leak detector is used to confirm that there are no leaks in the system. A vacuum leak causes the interfusion of water molecules, which may cause blocking of the nanopore entrances. As-synthesized porous coordination polymers usually have water molecules or organic solvent inside their nanopores. Before the measurement in gas adsorption, the water molecules or organic solvent must be removed from the nanopores. Using this system, the sample is easily degassed by heating the sample during evacuation. The sample of CPL-1 was degassed for approximately 10 min at 373 K to remove water molecules in the nanochannel. The removal of guest molecules was confirmed from the diffraction pattern. The gas import tube and a gas handling system were heated carefully using a heat gun. The oxygen was then introduced at 80 kPa at room temperature. The gas adsorption state can be controlled by the temperature of the sample and the gas pressure. In the measurement of gas adsorption isotherms, the gas pressure is changed under constant temperature. In the present study, since the amount of a powder sample is very small, i.e., less than a few milligrams, the temperature is better controlled than the gas pressure. Therefore, the adsorption state was controlled by the sample temperature under a constant gas pressure. The temperature of the sample was gradually lowered from 300 to 90 K in order to initiate the gas adsorption. In order to obtain an equilibrium state of sorption, the delay time was set to be from 5 to 10 min before each measurement. The measured *in situ* powder diffraction patterns of CPL-1 with the adsorption of oxygen at 80 kPa are shown in Fig. 2. Dramatic changes of the peak position and relative intensity of reflections are observed between 150 and 130 K. These changes are thought to be caused by the adsorption of oxygen. Gas adsorption isotherm is measured previous to the diffraction experiment in order to examine the entire gas adsorption profile. From the isotherm, oxygen molecules are thought to be adsorbed in CPL-1 until saturation at 90 K at a gas pressure of 80 kPa. By measurement with an exposure time of 5–10 min, the data were obtained with a counting statistic that was sufficient for atomic level structure analysis by the Rietveld method. Accurate charge density analysis requires reliable integrated intensities of Bragg reflection. In order to obtain a much higher counting statistic data, the exposure time is determined from the maximum limit of counting by an IP. The exposure time is estimated from a brief 5-min measurement. In the present case, the data for charge density analysis was measured with an exposure time of 65 min at 90 K. After this measurement, the sample was heated to 300 K and the diffraction pattern changed to that of CPL-1 without guest molecules. The desorption of oxygen and the recovery of hollow structure without a collapse of the framework of CPL-1 were confirmed.

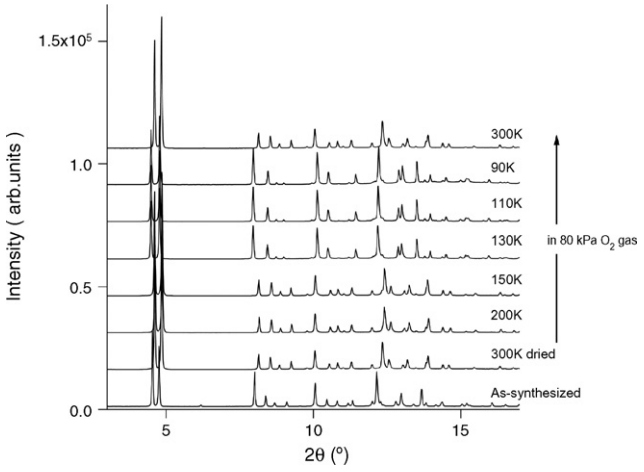


Fig. 2. *In situ* synchrotron powder diffraction patterns of CPL-1 with the adsorption of oxygen at 80 kPa. The diffraction pattern of as-synthesized CPL-1 is also shown. The wavelength of the incident X-ray is 0.8 Å.

## 3. Structural analysis by the MEM/Rietveld method

In the powder diffraction method, a three-dimensional intensity distribution of a reciprocal lattice is degenerated into one-dimensional data and a great deal of information on the integrated intensity of each reflection is lost. The X-ray diffraction provides the absolute values of the integrated intensities of each reflection and the phases cannot be essentially obtained. In the single-crystal X-ray diffraction method, there exists a direct method that can estimate the phases of each reflection. However, it is very difficult to estimate the phases by a powder method. In Rietveld analysis, the diffraction pattern calculated from the expected structural model is fitted to the observed pattern to refine some structural parameters by the least-squares method. It is important that the initial structural model is correct or close to the correct model and the initial parameters are close to the correct values. So the construction of the structural model is a key to the success of the analysis. In the present study, little structural information on adsorbed gas molecules is available at the beginning of the analysis. The position and orientation of guest molecules are not known. In such a case, if we assume the guest molecules to have arbitrary positions and refine their positional parameters, then the solution may fall into a local minimum and fail the analysis. Therefore, an enormous number of trials for various structural models must be performed. In order to avoid such difficulties, we apply the imaging technique of charge densities by the newly developed MEM to help in the model building of gas-adsorbed structures.

The MEM is a type of image reconstruction technique that was developed in the area of information theory and has been applied in the field of radio astronomy to reconstruct images from incomplete and noisy data [19]. The MEM was developed as a deconvolution method and was applied to crystal structure analysis in 1982 by Collins [13]. The MEM algorithm used in the present study is based on Collins' method. The MEM gives the high-resolution charge density distribution consistent with the crystal structure factors within the errors. In the calculation of the MEM, the information entropy based on the charge density distribution is maximized with the constraint concerning the agreement of observed and calculated structure factors. In 1995, the MEM combined with the most popular powder pat-

tern decomposition method, the Rietveld method, was developed for the determination of the endohedral structure of a metallofullerene. This method is known as the MEM/Rietveld method [15,16]. The MEM/Rietveld method is used for two types of applications in crystal structure analysis. One such application is accurate charge density analysis. The integrated intensities of each Bragg reflection are obtained using the result of powder pattern decomposition in Rietveld analysis. The resultant structure factors are used for the calculation of the MEM to obtain an accurate charge density. This is very useful for analyzing powder patterns with significant overlaps of reflections. By this method, the bonding natures of various materials, such as oxides [20,21], intermetallic compounds [22,23], and superconductors [24], were revealed. Another application is the model building and modification of the crystal structure by the combination of powder pattern decomposition and imaging of the charge density consistent with the diffraction data, which is referred to as structural prediction by the MEM. This method has provided a breakthrough in the structure determination of fullerene compounds [15,25–27]. Of course, an accurate charge density can be obtained after the model building.

A procedure of the structure analysis of a porous coordination polymer with the adsorption of molecular oxygen is shown as an example of model building by the MEM/Rietveld method. A diffraction pattern of CPL-1 with the adsorption of oxygen at a pressure of 80 kPa measured at 90 K is analyzed. The diffraction peaks of the sample are observed to have a broad halo pattern from the soda glass capillary. This background reflects the structure of the glass and is expressed by the combination of a number of broad peaks using a profile function. In the first step of analysis, the Rietveld refinement is carried out by a structural model of only the framework, without assuming any guest molecules inside the nanopores. Crystal structure of as-synthesized CPL-1 with water molecules in the nanochannels has already been determined by single-crystal X-ray diffraction [3]. From the similar diffraction pattern of as-synthesized CPL-1, the crystal system of CPL-1 with the adsorption of oxygen is expected to be a monoclinic. We assume that the fundamental framework structure of CPL-1 does not change by the gas adsorption. The structural model of the framework is made by the removal of water molecules from the structural model of the as-synthesized compound. In the refinement of atomic coordinates, pyrazine molecules and carboxylate forming the framework are treated as rigid bodies so as to maintain their intrinsic forms. The soft-constraints for intermolecular distances and the angles of these components of the framework are appropriately applied in the refinement. The result of this Rietveld fitting is shown in Fig. 3(a). The data of $2\theta \leq 53.3^\circ$, which correspond to $d \geq 0.89$ Å$^{-1}$, were used in the analysis. The calculated peak positions of each reflection showed good agreement with those of the observed data and the fundamental structure of the framework was confirmed to have a monoclinic cell. The fitting of the observed and calculated powder patterns is very bad due to the lack of guest gas molecules in the present structural model. Reliability factors based on the entire powder profile, $R_{wp}$, and the Bragg integrated intensities, $R_I$, were 16.4 and 44.9%, respectively. Despite the unsatisfactory fitting of data,

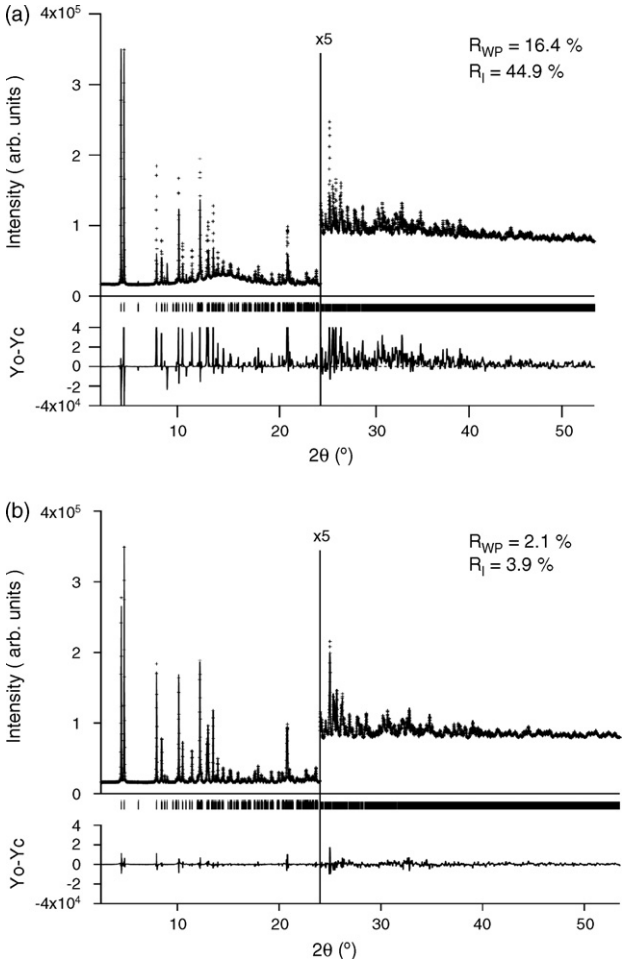


Fig. 3. Fitting results of Rietveld refinement for CPL-1 with the adsorption of oxygen. (a) Initial refinement using a structural model of CPL-1 framework without guest molecules. (b) Final refinement using the modified structural model of CPL-1 with oxygen.

the integrated intensities of each reflection were derived from the observed diffraction patterns using the result of the Rietveld refinement. The diffraction intensity of each data point is divided into each reflection with the contribution from each reflection using the proportion of the calculated intensities in accordance with the following equation:

$$Y_i^{\mathrm{obs}}(2\theta_j) = Y^{\mathrm{obs}}(2\theta_j) \times \frac{Y_i^{\mathrm{calc}}(2\theta_j)}{\sum_i^N Y_i^{\mathrm{calc}}(2\theta_j)} \quad (1)$$

where $Y^{\mathrm{obs}}(2\theta_j)$ is the observed diffraction intensity at $2\theta_j$ and has contributions from $N$ reflections, $Y_i^{\mathrm{calc}}(2\theta_j)$ the calculated intensity from the structural model in the Rietveld analysis for the $i$th reflection at $2\theta_j$, and $Y_i^{\mathrm{obs}}(2\theta_j)$ is the contribution from the $i$th reflection at $2\theta_j$. This operation is carried out for all data points. As a result, all of the observed intensities are divided into each reflection without exception, and the integrated intensities of each reflection based on the observed data are obtained. From the statistical consideration, the standard deviation of integrated intensity is estimated to be the square root of the integrated intensity. The structure factors of each reflection are derived from these integrated intensities. The phases of structure fac-

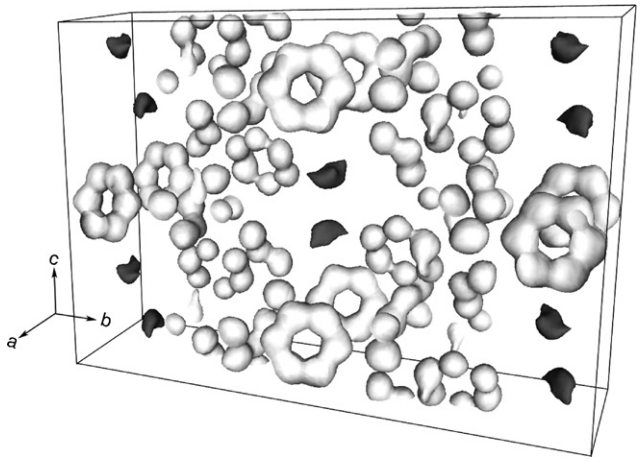


Fig. 4. Three-dimensional MEM charge density map of CPL-1 with the adsorption of oxygen as equi-contour surfaces based on the first Rietveld analysis using the structural model without assuming guest molecules. The equi-density level is 0.8 eÅ$^{-3}$. Distributions in the nanochannel are indicated in black.

tors calculated from the structural model are given. Imaging of the charge density by the MEM is performed using resultant structure factors. The MEM calculation was carried out using the ENIGMA program [28]. In the MEM calculation, the unit cell is divided into 64 × 256 × 128 pixels. The total number of electrons in the unit cell is given as a constraint. The number of adsorbed gas molecules is included in this calculation. The amount of adsorbed gas molecules is independently examined by the gas adsorption isotherm. In this analysis, one $O_2$ molecule is adsorbed for one formula unit. Fig. 4 shows an obtained three-dimensional MEM charge density map as equi-contour surfaces. The framework structure can be clearly seen. Despite the structural model without assuming guest molecules, two peaks of charge density are recognized in each pore. Fig. 5(a) shows a section MEM charge density containing this peak, which is parallel to the nanochannel direction. The middle of this figure corresponds to the nanochannel. An elongated shape distribution of charge density is seen in the middle of the nanochannel. Although the adsorbed molecules are not assumed in the structural model in this analysis, the diffraction intensities must

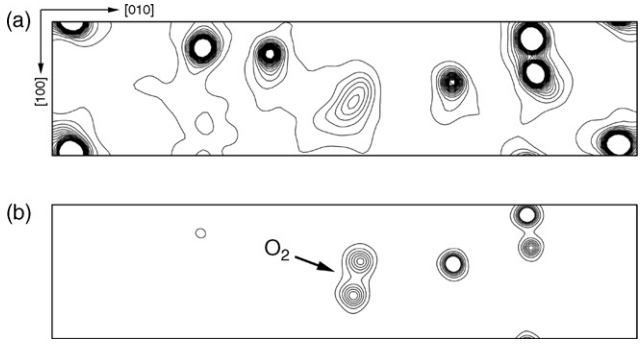


Fig. 5. Section MEM charge density maps containing a nanochannel for CPL-1 with the adsorption of oxygen. (a) MEM charge density based on the first Rietveld analysis. Contour lines are drawn from 0.0 to 4.0 eÅ$^{-3}$ with 0.2 eÅ$^{-3}$ intervals. (b) Final MEM charge density based on the Rietveld analysis using the modified structural model. Contour lines are drawn from 0.0 to 14.0 eÅ$^{-3}$ at 2.0 eÅ$^{-3}$ intervals.

contain the information of the adsorbed molecules. The information was derived by imaging of the charge density consistent with input data by the MEM. The charge density in the middle of the nanochannel is thought to be due to the adsorbed $O_2$ molecule.

As the next step in the analysis, the modified structural model with $O_2$ molecules at the peak positions of charge density in the nanochannel is applied as a new model to perform the Rietveld refinement again. The positional and orientation parameters of $O_2$ molecules were also refined in this analysis. The results of the final Rietveld refinement are shown in Fig. 3(b), which indicates a satisfactory fitting. Reliability factors $R_{WP}$ and $R_I$ were dramatically improved to 2.1 and 3.9%, respectively. If the obtained MEM charge density distribution is consistent with the structural model used in the Rietveld model, it is considered as a final result. Fig. 5(b) shows that a section MEM charge density contains the $O_2$ molecule, which is parallel to the nanochannel direction. Through the use of the modified structural model, the charge density distribution of the $O_2$ molecule became dumbbell shaped. The feature of the obtained MEM charge density is consistent with the structural model used in Rietveld refinement at the atomic level and is a final result of this analysis.

As shown here, the MEM/Rietveld method, which is combined with the ability of the structure model prediction of the MEM and the powder pattern decomposition of the Rietveld method, was shown to be very useful for the structural determination of porous coordination polymers with the gas adsorption. This method is also powerful for the structure determination of the rotational or positional disorder of molecules and organic ligands for which their structural model is difficult to express and build.

## 4. Molecular arrangement of oxygen and nitrogen in CPL-1

The dioxygen molecule is paramagnetic. The low-dimensional arrangement of molecular oxygen makes the investigation of the intermolecular potential and the quantum effect on magnetic properties very attractive. Gas adsorption on the nanopores of coordination polymers is a promising method by which to realize such an arrangement of molecular oxygen. In the present study, the host-guest interaction between $O_2$ molecules and the nanopore and the guest–guest interaction between the adsorbed $O_2$ molecules is investigated. In this section, the molecular arrangement of oxygen adsorbed in the nanochannels of porous coordination polymers, called CPL-1, and that of nitrogen, which has a similar size and shape to oxygen, are shown.

CPL-1 has a pillared-layer structure. Two-dimensional sheets composed of copper and pyrazine-2,3-dicarboxylate are linked by pyrazine molecules, forming uniform ordered nanochannels. The size of the nanochannel is similar to that of molecular oxygen. The oxygen adsorption isotherm on CPL-1 at 77 K is a typical profile of a type 1 isotherm, with a steep rise at the low-pressure region, which is characteristic of the adsorption on micropores. The adsorption is expected to achieve saturation at 90 K and 80 kPa. The temperature dependence of the lattice

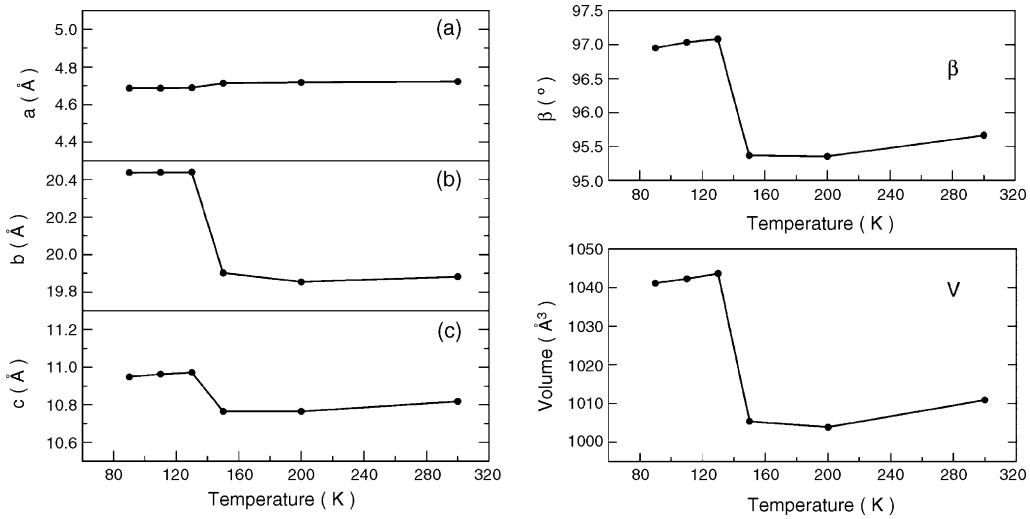


Fig. 6. Temperature dependence of lattice parameters and the unit cell volume of CPL-1 with the adsorption of oxygen.

parameters of CPL-1 with the adsorption of oxygen is shown in Fig. 6. Whereas most lattice parameters and the cell volume increased between 150 and 130 K by the adsorption of oxygen, a small change in the direction of the nanochannel was observed. Fig. 7 shows the three-dimensional MEM charge density of CPL-1 with the adsorption of oxygen as equi-contour surfaces. A reliability factor based on the structure factors $R_{FMEM}$ is 1.51%. The host framework structure is clearly seen in this map. Two peaks of electron density are observed in each unit pore of CPL-1, which is consistent with the result of the adsorption isotherm. A unit pore is defined as one pore between two pillar-ligand pyrazine molecules as viewed from the nanochannel direction. Each molecule has the dumbbell-shaped distribution of the $O_2$ molecule. The number of electrons around this peak as calculated from the MEM charge density was 15.8(1)e. This value virtually agrees with the number of electrons of the neutral $O_2$ molecule. It was confirmed by X-ray structure analysis for the first time that the molecular oxygen is adsorbed in the nanochannels of porous coordination polymer. The $O_2$ molecule is located in the middle of the nanochannel. No electron density showing chemical bonding is seen between the adsorbed $O_2$ molecule and the pore walls. The interatomic distances between the $O_2$ molecule and the atoms on the pore walls are from approximately 2.7 to 3.3 Å, which shows the van der Waals contact of these atoms. These observations support that idea that $O_2$ molecules are physisorbed in the nanochannels of CPL-1. A parameter of isotropic temperature factor $B$ was refined to be 4.1 $Å^2$, this large value shows that the $O_2$ molecules have large thermal vibration in the nanochannels. However, a clear charge density distribution of adsorbed $O_2$ molecule shows that the molecules are strongly trapped at this position. The state of the oxygen in the nanochannels is thought to be closer to a solid state than a liquid state. As shown here, the MEM charge density distribution provides information on the molecular interaction, i.e., the charge transfer between the molecules and ionicity of atoms, because it is calculated for all of the electrons in the system.

Fig. 8 shows the arrangement of the $O_2$ molecule in the nanochannel of CPL-1. Adsorbed $O_2$ molecules form a ladder structure. The intermolecular distance of the $O_2$–$O_2$ dimer is 3.28 Å, which is close to that in the $\alpha$ and $\beta$ phases of solid

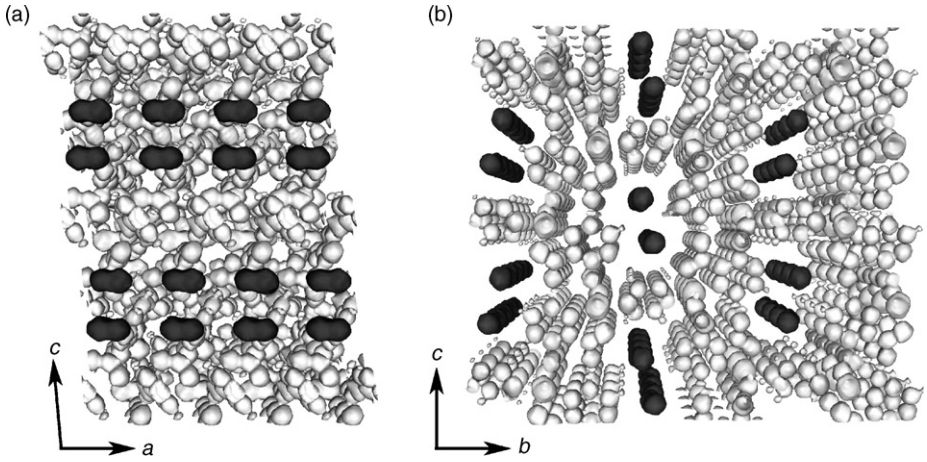


Fig. 7. Three-dimensional MEM charge density of CPL-1 with the adsorption of oxygen as equi-contour surfaces viewed from (a) the side and (b) the front of the nanochannels. The equi-density level is 1.0 $eÅ^{-3}$. Adsorbed $O_2$ molecules are indicated in black.

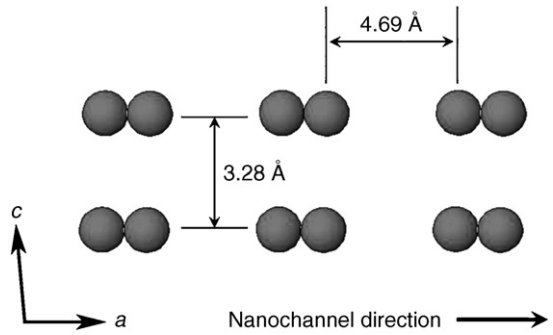


Fig. 8. Arrangement of $O_2$ molecules in the nanochannel of CPL-1 viewed from the side of the nanochannel direction.

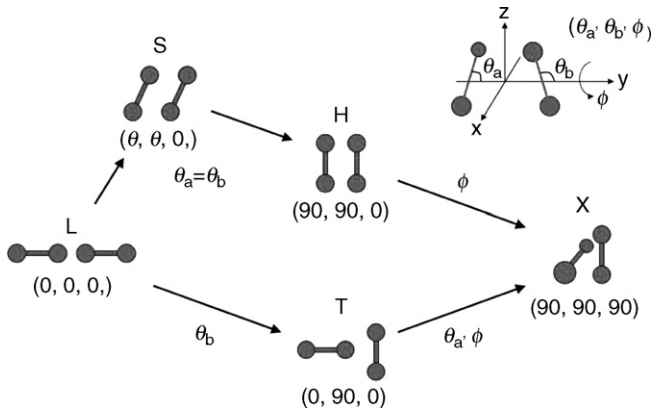


Fig. 9. Geometries of the dimer system.

$O_2$. On the other hand, the interdimer distance of 4.69 Å, as determined by the lattice parameter of the framework, is relatively large. Theoretical studies have shown that the magnetic interaction between $O_2$ molecules strongly depends on the intermolecular distance and the orientation of the molecular axis [29]. These results indicate that the interdimer interaction is approximately hundred times weaker than the intradimer interaction. Therefore, the magnetic properties of this system are assumed to be equivalent to those for a Heisenberg antiferromagnetic dimer with $S = 1$. The experimental results were published in Refs. [30] and [31]. The temperature dependence of the susceptibility and the high-field magnetization process at low temperatures indicate the non-magnetic singlet ground state of the $O_2$–$O_2$ dimer. In the magnetization process at 4.2 K, the magnetization contribution from adsorbed $O_2$ increases abruptly at approximately 60 T, although the present magnetic field is not sufficient to obtain the saturated magnetization. Similar metamagnetic-like behavior has been observed in two other microporous coordination polymers [30]. We recently proposed the "field-induced rearrangement mechanism" as an explanation for the metamagnetic-like behavior. The stable arrangement of $O_2$ with saturated magnetic moment in a sufficiently high field should be different from the H-structure in the singlet state, which is stable at zero field. The geometries of the dimer system are shown in Fig. 9. Therefore, the magnetization process of the $O_2$–$O_2$ dimer is expected to be different from that of the $S = 1$ Heisenberg antiferromagnetic dimer model.

A CPL-1 with adsorbed nitrogen was investigated using the same type of experiment and analysis for comparison with the adsorption of oxygen [31]. The nitrogen molecule has a size similar to that of oxygen and is a good reference for studying the differences in interaction between the adsorbed molecules and nanopores. The gas pressure of nitrogen in the *in situ* powder diffraction experiment was 80 kPa. The measurement time of data for charge density analysis was 90 min. From the change of the *in situ* diffraction pattern, nitrogen was found to be adsorbed between 130 and 120 K. This is consistent with the higher saturated vapor pressure of nitrogen, as compared to oxygen. Reliability factors $R_{WP}$ and $R_I$ in the final Rietveld refinement were 1.81 and 3.84%, respectively. An isotropic thermal parameter, $B$, was refined to be 4.8 Å$^2$. The refined lattice parameters and the unit cell volume of CPL-1 with the adsorption of nitrogen and oxygen, and without guest molecules, are shown in Table 1. The crystal lattice mainly expands in the direction of the $b$ and $c$ axes, which indicates the expansion of the nanopore by the gas adsorption. A slight contraction is seen in the $a$ axis, which is the nanochannel direction. These tendencies are similar for the case of oxygen adsorption and nitrogen adsorption. Fig. 10 shows the three-dimensional MEM charge density of CPL-1 with the adsorption of nitrogen as equi-contour surfaces. The reliability factor $R_{FMEM}$ is 2.21%. The dumbbell-shaped charge density due to the adsorbed $N_2$ molecules is observed in the middle of nanochannels. The interatomic distance between adjacent $N_2$ molecules is 3.61 Å. The nitrogen molecules aligned to the nanochannel direction, forming dimers. No electron density distribution or charge transfer was observed between the $N_2$ molecules and pore walls. These features are very similar to those in the oxygen adsorption. However, in the case of nitrogen adsorption, the molecular axis of the $N_2$ molecule was inclined 24.9° to the nanochannel direction. The $N_2$–$N_2$ dimer has a shifted parallel S-structure ($\theta_a = \theta_b \neq 90°$). The difference of the arrangement of adsorbed molecules between oxygen and nitrogen is considered to arise from the intermolecular inter-

Table 1
The refined lattice parameters and the unit cell volume of CPL-1 with the adsorption of nitrogen and oxygen, and without guest molecules at 90 K

| | $P$ (kPa) | $a$ (Å) | $b$ (Å) | $c$ (Å) | $\beta$ (°) | $V$ (Å$^3$) |
|---|---|---|---|---|---|---|
| With oxygen[a] | 80 | 4.68759 (4) | 20.4373 (1) | 10.94837 (9) | 96.9480 (6) | 1041.17(1) |
| With nitrogen[b] | 80 | 4.6965 (1) | 20.5432 (2) | 11.0320(1) | 97.451 (2) | 1055.39(3) |
| Without guest molecules[c] | 0 | 4.7154(1) | 19.8268 (2) | 10.7124(2) | 95.065(2) | 997.60 (3) |

[a] From Ref. [17].
[b] From Ref. [31].
[c] From Ref. [32].

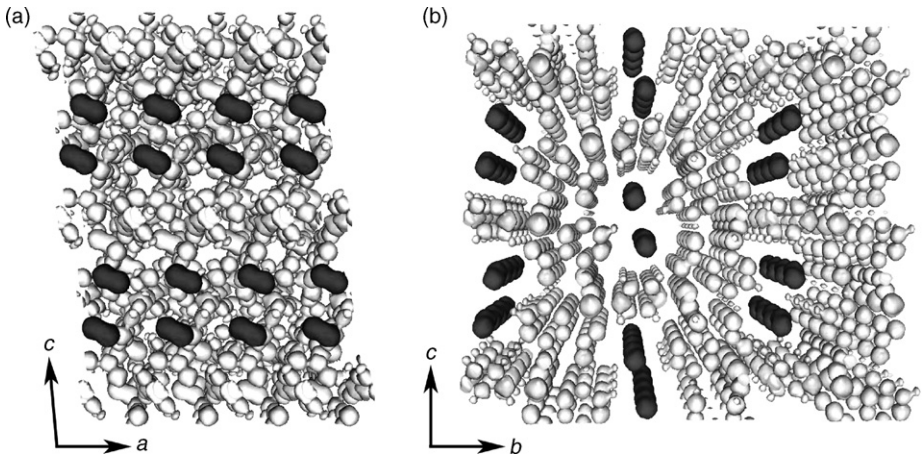


Fig. 10. Three-dimensional MEM charge density of CPL-1 with the adsorption of nitrogen as equi-contour surfaces viewed from (a) the side and (b) the front of the nanochannels. The equi-density level is 1.0 $e\text{Å}^{-3}$. Adsorbed $N_2$ molecules are indicated in black.

action between the guest molecules. These considerations are discussed later in Section 7.

## 5. High-pressure synchrotron powder diffraction experiment of gas adsorption

A gas adsorption state can be controlled by the temperature and the gas pressure. An *in situ* powder diffraction gas adsorption experiment at BL02B2 was carried out by controlling the temperature under a constant gas pressure because of the condition whereby a small amount of sample can be easily and accurately controlled by temperature. Gas molecules can also be compulsorily adsorbed inside the nanopores by applying pressure. This procedure is performed in an *in situ* experiment under high pressure. The molecular alignment of oxygen adsorbed under high pressure may be different from that at low temperature at a pressure of 80 kPa. The framework of CPL-1 is expected to transform with increasing pressure. The molecular alignment is related to the valance of the interaction between the adsorbed molecules and the pore walls and that between the adsorbed molecules. The arrangement of dimers of oxygen and their magnetic properties are of interest here. In this section, the pressure induced molecular alignment of oxygen and the transformation of CPL-1 framework are shown.

An *in situ* powder diffraction experiment of gas adsorption under high pressure was carried out by high-pressure research beamline BL10XU SPring-8 [33]. An X-ray obtained by an in-vacuum undulator was monochromatized by a Si (1 1 1) double crystal. The wavelength of the incident X-ray was 0.49 Å. Diffraction patterns were measured by a Rigaku R-AXIS IV, using a flat imaging plate of 300 mm × 300 mm in size as a detector. The camera distance was approximately 300 mm. In order to produce a high-pressure condition, a diamond anvil cell (DAC) was used. The amount of powder sample placed into the DAC is very small, which enables homogeneity of pressure. Thus, a high-brilliance and high-resolution synchrotron radiation light source is indispensable for the diffraction experiment with a DAC. In order to obtain a hydrostatic pressure, helium gas is often used as a pressure medium placed into the DAC together with the powder sample [34]. In this experiment, oxygen that should be adsorbed in the sample of a porous coordination polymer was used as a pressure medium. Liquid oxygen was dosed into a DAC with powder sample of CPL-1 under liquid nitrogen temperature. A small ruby crystal was placed together with the powder sample. The pressure in the DAC was monitored by the shift of fluorescence spectrum of the ruby. An incident X-ray beam is irradiated through the diamond, and the diffracted beam from the sample passes through the diamond to reach the detector. The measurement was performed at room temperature. The gas pressure was changed from 0.26 to 8.03 GPa. The exposure time for each diffraction data was set to be 5 min. The one-dimensional powder diffraction pattern was obtained from the recorded two-dimensional IP data by the software PIP [35]. Fig. 11 shows the pressure dependence of the powder diffraction patterns of CPL-1 with the adsorption of oxygen. The peak positions gradually change with increasing pressure. The shifts of the peak positions in each diffraction pattern differ with the type of reflection. Some peaks do not shift much. This indicates the occurrence of an anisotropic deformation of crystal lattice with increasing pressure. The pressure dependence of the lattice

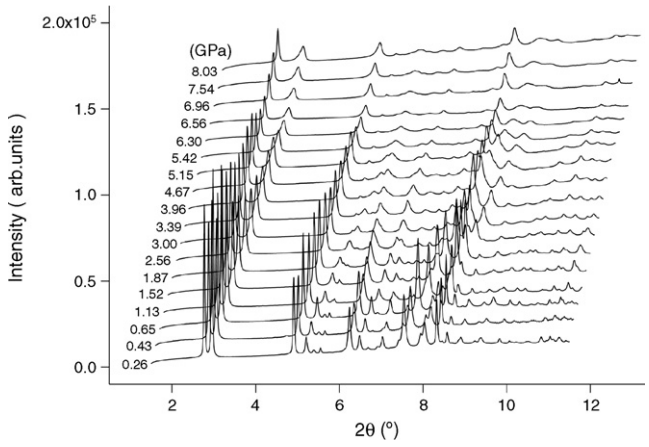


Fig. 11. Pressure dependence of synchrotron powder diffraction patterns of CPL-1 with the adsorption of oxygen. Each profile is offset in the direction of the horizontal and vertical axes to avoid overlapping.

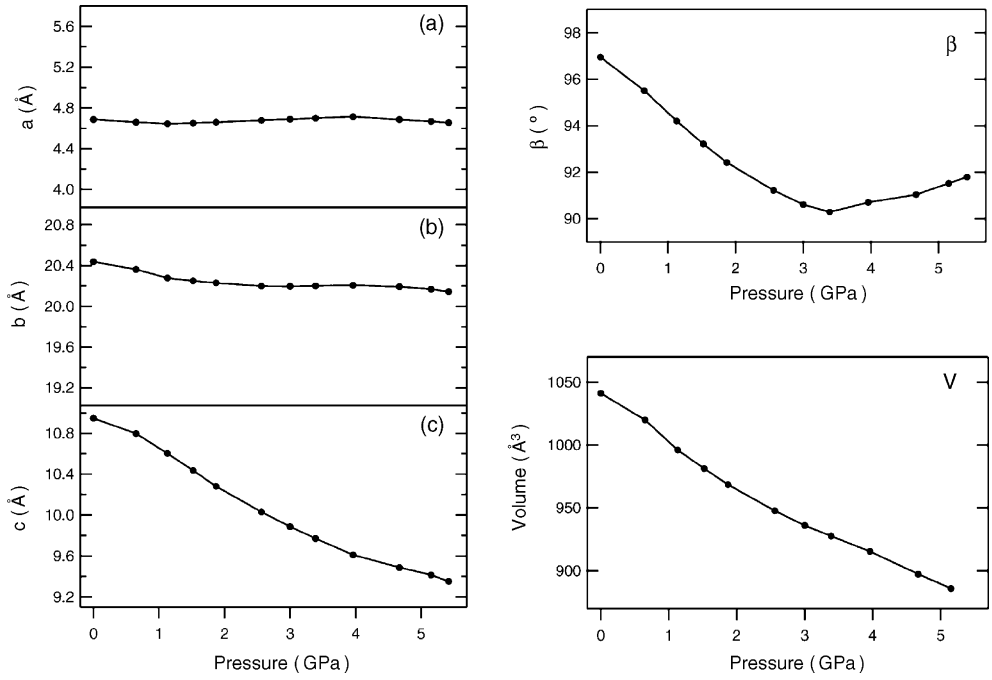


Fig. 12. Pressure dependence of lattice parameters and the unit cell volume of CPL-1 with the adsorption of oxygen.

parameters and the unit cell volume obtained from the Le Bail analysis is shown in Fig. 12. The lattice was found to contract mainly in the direction of the *c* axis with increasing pressure. On the other hand, a small change is seen in the direction of the nanochannel. The volume change of the crystal lattice within the observed pressure range was approximately 7%. The diffraction profiles become broader in the higher pressure region due to the failing of crystallinity. The Rietveld analysis was carried out for the data of the pressure range of from 0.65 to 1.87 GPa with sharp diffraction profiles.

## 6. Pressure-induced molecular arrangement of oxygen

Fig. 13 shows the pressure dependence of the crystal structure of CPL-1 with the adsorption of oxygen. A crystal structure at 80 kPa and 90 K is also shown in this figure. At 80 kPa, the molecular axis of oxygen was parallel to the nanochannel, and the dimers have an H-structure forming a ladder structure. From the structural analysis, the molecular axis of the $O_2$ molecule was found to be gradually inclined for the nanochannel direction with increasing pressure. The $O_2$–$O_2$ dimers seem to change their orientation, maintaining an H-structure in this pressure region. Pillar ligand pyrazine molecules also rotated with increasing pressure. A plane of the pyrazine molecule became perpendicular to the nanochannel direction. The lattice parameters *c* and $\beta$ simultaneously decreased to show the lattice shearing. One of the most interesting results is the increase of lattice parameter $\beta$ above 3 GPa, as shown in Fig. 12. The structural changes that occur and the arrangement of the $O_2$ dimer in this pressure region should be analyzed in the future. From the preliminary MEM charge density analysis, little charge density was observed between the $O_2$ molecules and pore walls. This indicates that the $O_2$ molecules are basically physisorbed in the nanochannels of CPL-1, as at 80 kPa and 90 K. The transformation with the lattice shearing and the rotation of pyrazine molecules seems to attain a denser structure to generate an efficient guest accommodation.

## 7. $O_2$–$O_2$ dimers in the nano-coordination space of CPL-1

Based on the determined crystal structures of CPL-1 with oxygen and nitrogen, adsorbed gas molecules are thought to be affected by the potential, depending on the shape of the pore surfaces, to form ordered structures in nanochannels. Neither charge densities showing chemical bonds nor charge transfers were observed between the adsorbed guest molecules and the pore walls in the MEM charge densities. The interaction between the guest molecules and the pore wall is thought to be due to van der Waals force. The experimental results of the different arrangement of the $O_2$–$O_2$ dimer and the $N_2$–$N_2$ dimer strongly suggest that the guest-guest interaction plays an essential role in the determination of the molecular arrangement. Considering the interaction of the quadrupolar moment of $N_2$ molecules, the stable arrangement of the free dimer is expected to have a T-structure or a shifted parallel S-structure. However, the T-structure cannot be attained because of the restricted space inside the nanochannels of CPL-1. Therefore, the $N_2$–$N_2$ dimer has an S-structure with $\theta = 65.1^\circ$ in the nanochannels. The situation for the $O_2$–$O_2$ dimer is different from that of the $N_2$–$N_2$ dimer because of the existence of the magnetic interaction. The results of a theoretical study [29] and a molecular beam experiment [36] indicate that the most stable geometry of a singlet $O_2$–$O_2$ dimer with $S = 0$ is expected to have an H shape. The geometry in solid $\alpha$ and $\beta$ phases of oxygen is an H shape and the interaction between the molecules is antiferromagnetic. The $O_2$–$O_2$ dimers at 80 kPa and 90 K have an H-structure. Below 90 K, they are thought

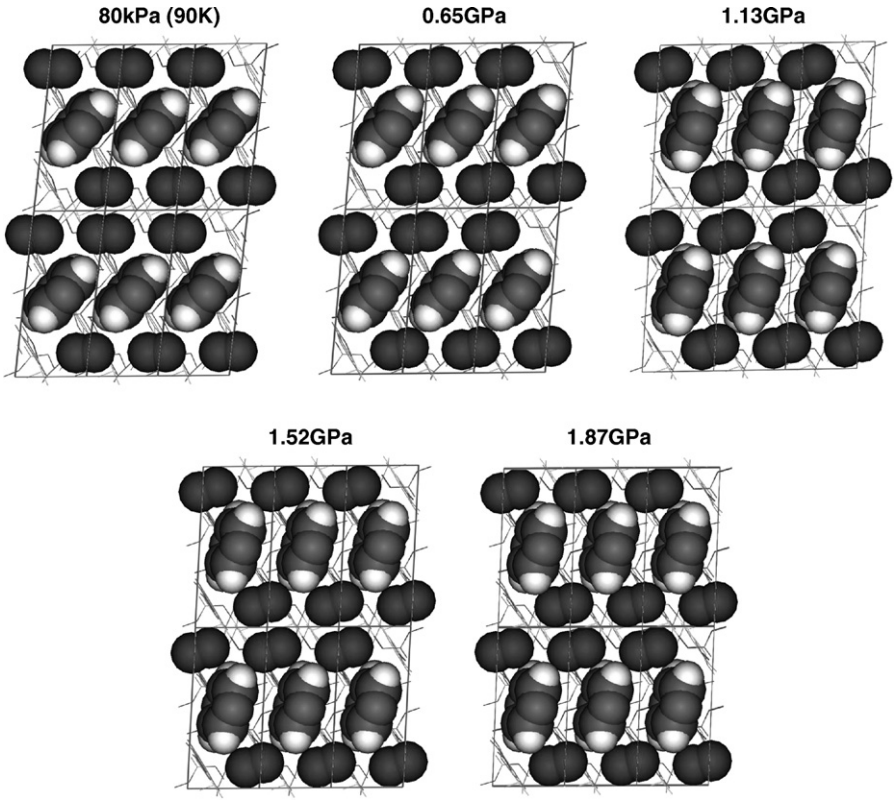


Fig. 13. Pressure dependence of the crystal structure of CPL-1 with the adsorption of oxygen. These figures are viewed from the side of the nanochannel direction. Adsorbed oxygen dimers and pillar ligand pyrazine molecules are shown by the space-filling model. Others are shown by connecting lines.

to maintain an H-structure from the non-magnetic behavior in susceptibility measurement. The H-structure is also maintained under high pressure despite the expected enhancement of the host-guest interaction. Robust H-structure under high pressure may indicate the importance of the guest–guest interaction.

## 8. Conclusions

Gas molecules adsorbed in the nanochannels of porous coordination polymer were directly observed by the combination of an *in situ* powder diffraction experiment of gas adsorption using a third-generation synchrotron radiation light source. Imaging of the charge density by the MEM provided information on the adsorbed gas molecules, enabling the structural model to be built and modified. The structure obtained, not only the atomic positions, but also the charge density distribution, indicated that the arrangement of dimers and their specific states differed from the bulk state in the nano-coordination space.

## Acknowledgements

This study was supported by the Ministry of Education, Culture, Sports, Science and Technology of Japan through a Grant-In-Aid for Scientific Research in a Priority Area 'Chemistry of Coordination Space' and by CREST/JST and JASRI/SPring-8 Nanotechnology Support Project of the Ministry of Education, Culture, Sports, Science and Technology of Japan. The authors would like to thank Drs. R. Kitaura and R. Matsuda of Kyoto University for the syntheses of samples and valuable discussions, Drs. K. Kato, K. Osaka, T. Adachi, and Y. Ohishi of JASRI, and Dr. Y. Akahama of the University of Hyogo, for their kind advice and assistance in data collection. The authors would also like to thank Dr. H. Tanaka of Shimane University for use of the ENIGMA computer program for the MEM analysis. Finally, the authors would like to thank Prof. M. Sakata of Nagoya University for providing valuable discussions.

## References

[1] O.M. Yaghi, M. O'Keeffe, N.W. Ockwig, H.K. Chae, M. Eddaoudi, J. Kim, Nature 423 (2003) 705.
[2] S. Kitagawa, R. Kitaura, S. Noro, Angew. Chem. Int. Ed. Engl. 43 (2004) 2334.
[3] M. Kondo, T. Okubo, A. Asami, S. Noro, T. Yoshitomi, S. Kitagawa, T. Ishii, H. Matsuzaka, K. Seki, Angew. Chem. Int. Ed. Engl. 38 (1999) 140.
[4] C.J. Kepert, M.J. Rosseinsky, Chem. Commun. (1999) 375.
[5] M. Kondo, M. Shimamura, S. Noro, S. Minakoshi, S. Asami, K. Seki, S. Kitagawa, Chem. Mater. 12 (2000) 1288.
[6] X. Zhao, B. Xiao, A.J. Fletcher, K.M. Thomas, D. Bradshaw, M.J. Rosseinsky, Science 306 (2004) 1012.
[7] G. Férey, M. Latroche, C. Serre, F. Millange, T. Loiseau, A. Percheron-Guégan, Chem. Commun. (2003) 2976.
[8] D.N. Dybtsev, H. Chun, S.H. Yoon, D. Kim, K. Kim, J. Am. Chem. Soc. 126 (2004) 32.
[9] J.L.C. Rowsell, A.R. Millward, K.S. Park, O.M. Yaghi, J. Am. Chem. Soc. 126 (2004) 5666.
[10] S. Noro, S. Kitagawa, M. Kondo, K. Seki, Angew. Chem. Int. Ed. Engl. 39 (2000) 2082.
[11] B.F. Hoskins, R. Robson, J. Am. Chem. Soc. 112 (1990) 1546.

[12] M. Fujita, Y.J. Kwon, S. Washizu, K. Ogura, J. Am. Chem. Soc. 116 (1994) 1151.
[13] D.M. Collins, Nature 298 (1982) 49.
[14] M. Sakata, M. Sato, Acta Crystallogr. A 46 (1990) 263.
[15] M. Takata, B. Umeda, E. Nishibori, M. Sakata, Y. Saito, M. Ohno, H. Shinohara, Nature 377 (1995) 46.
[16] M. Takata, E. Nishibori, M. Sakata, Z. Kristallogr. 216 (2001) 71.
[17] R. Kitaura, S. Kitagawa, Y. Kubota, T.C. Kobayashi, K. Kindo, Y. Mita, A. Matsuo, M. Kobayashi, H. Chang, T.C. Ozawa, M. Suzuki, M. Sakata, M. Takata, Science 298 (2002) 2358.
[18] M. Takata, E. Nishibori, K. Kato, Y. Kubota, Y. Kuroiwa, M. Sakata, Adv. Xray Anal. 45 (2002) 377.
[19] S.F. Gull, G.L. Daniel, Nature 272 (1978) 686.
[20] M. Takata, E. Nishibori, K. Kato, M. Sakata, Y. Moritomo, J. Phys. Soc. Jpn. 68 (1999) 2190.
[21] Y. Kuroiwa, S. Aoyagi, A. Sawada, J. Harada, E. Nishibori, M. Takata, M. Sakata, Phys. Rev. Lett. 87 (2001) 217601.
[22] Y. Kubota, M. Takata, M. Sakata, T. Ohba, K. Kifune, T. Tadaki, J. Phys. Condens. Matter 12 (2000) 1253.
[23] K. Kirihara, T. Nakata, M. Takata, Y. Kubota, E. Nishibori, K. Kimura, M. Sakata, Phys. Rev. Lett. 85 (2000) 3468.
[24] E. Nishibori, M. Takata, M. Sakata, H. Tanaka, T. Muranaka, J. Akimitsu, J. Phys. Soc. Jpn. 70 (2001) 2252.
[25] M. Takata, E. Nishibori, B. Umeda, M. Sakata, E. Yamamoto, H. Shinohara, Phys. Rev. Lett. 78 (1997) 3330.
[26] E. Nishibori, M. Takata, M. Sakata, A. Taninaka, H. Shinohara, Angew. Chem. Int. Ed. Engl. 40 (2001) 2998.
[27] C. Wang, T. Kai, T. Tomiyama, T. Yoshida, Y. Kobayashi, E. Nishibori, M. Takata, M. Sakata, H. Shinohara, Nature 408 (2000) 426.
[28] H. Tanaka, M. Takata, E. Nishibori, K. Kato, T. Iishi, M. Sakata, J. Appl. Crystallogr. 35 (2002) 282.
[29] B. Bussery, S.Y. Umanskii, M. Aubert-Frécon, O. Bouty, J. Chem. Phys. 101 (1994) 416.
[30] T.C. Kobayashi, A. Matsuo, M. Suzuki, K. Kindo, R. Kitaura, R. Matsuda, S. Kitagawa, Prog. Theor. Phys. Suppl. 159 (2005) 271.
[31] R. Kitaura, R. Matsuda, Y. Kubota, S. Kitagawa, M. Takata, T.C. Kobayashi, M. Suzuki, J. Phys. Chem. B 109 (2005) 23378.
[32] Y. Kubota, M. Takata, R. Matsuda, R. Kitaura, S. Kitagawa, K. Kato, M. Sakata, T.C. Kobayashi, Angew. Chem. Int. Ed. Engl. 44 (2005) 920.
[33] M. Sakata, T. Itsubo, E. Nishibori, Y. Moritomo, N. Kojima, Y. Ohishi, M. Takata, J. Phys. Chem. Solids 65 (2004) 1973.
[34] K. Takemura, P.Ch. Sahu, Y. Kunii, Y. Toma, Rev. Sci. Instrum. 72 (2001) 3873.
[35] H. Fujihisa, K. Aoki, Rev. High Press. Sci. Technol. 8 (1998) 4.
[36] V. Aquilanti, D. Ascenzi, M. Bartolomei, D. Cappelletti, S. Cavalli, M.C. Vitores, F. Pirani, J. Am. Chem. Soc. 121 (1999) 10794.